ACS Photonics

Article

Cite This: ACS Photonics XXXX, XXX, XXX−XXX

Spectrally Selective Mirrors with Combined Optical and Thermal Benefit for Photovoltaic Module Thermal Management

Ian M. Slauch,[†] Michael G. Deceglie,[‡] Timothy J Silverman,[‡] and Vivian E. Ferry*[,†]

[†]Department of Chemical Engineering and Materials Science, University of Minnesota, 421 Washington Avenue SE, Minneapolis, Minnesota 55455, United States

[‡]National Renewable Energy Laboratory, Golden, Colorado, United States

Supporting Information

ABSTRACT: Waste heat generated during daytime operation of a solar module will raise its temperature and reduce cell efficiency. In addition to thermalization and carrier recombination, one major source of excess heat in modules is the parasitic absorption of light with sub-bandgap energy. Parasitic absorption can be prevented if sub-bandgap radiation is reflected away from the module. We report on the design considerations and projected changes to module energy yield for photonic reflectors capable of reflecting a portion of sub-bandgap radiation while maintaining or improving transmission of light with energy greater than the semiconductor bandgap. Using a previously developed, self-consistent opto-electro-thermal finite-element simulation, we calculate the total additional energy generated by a module, including various photonic reflectors, and decompose these benefits into thermal and optical effects. We show that the greatest total energy yield improvement comes from photonic mirrors designed for the outside of the glass, but that mirrors placed between the glass and the encapsulant can have significant thermal benefit. We then show that optimal photonic mirror design requires consideration of all angles of incidence, despite unequal amounts of radiation arriving at each angle. We find that optimized photonic mirrors will be omnidirectional in the sense that they have beneficial performance, regardless of the angle of incidence of radiation. By fulfilling these criteria, photonic mirrors can be used at different geographic locations or different tilt angles than their original optimization conditions with only marginal changes in performance. We show designs that improve energy output in Golden, Colorado by 3.7% over a full year. This work demonstrates the importance of considering real-world irradiance and weather conditions when designing optical structures for solar applications.

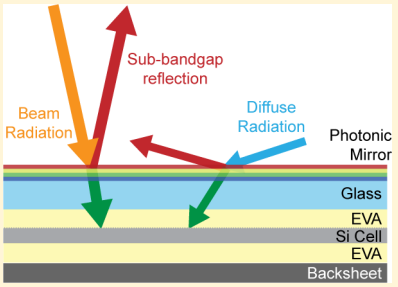

KEYWORDS: *photonic structures, solar cells, solar energy, cooling, photovoltaic modules, omnidirectional light transmission and reflection*

A typical crystalline Si solar module will operate 20−30 K above ambient temperature under sunny conditions while converting ∼20% of the incident solar energy to electricity.[1] Heat is produced within the module due to thermalization of carriers to the band edge, carrier recombination, ohmic loss, and parasitic sub-bandgap absorption. Elevated module operating temperature decreases the efficiency of a Si solar cell by ∼0.4% per 1 K, primarily due to a decrease in the open circuit voltage.[2] A number of strategies based on active and passive methods for solar module cooling have been proposed to mitigate this problem,[3−15] including optical designs to reflect sub-bandgap radiation or to increase the emissivity in the mid-infrared range and therefore enhance radiative cooling of the module.[16−19] We focus here on the reduction of parasitic absorption via reflection of sub-bandgap photons, as calculations have indicated that this strategy may lead to greater performance gains than tailored emissivity, which is limited by the already high emissivity of the module cover glass.[1,16,20]

For Si modules (bandgap ∼1.1 eV), ∼19% of solar radiation is below the bandgap energy and could be reflected away with a photonic mirror.[1] Increased reflection prevents this light from entering the module, decreasing the module temperature and therefore increasing energy output due to the thermal improvement. However, the ideal photonic mirror would not only reflect sub-bandgap radiation, but also transmit radiation at energies higher than the bandgap to maintain or improve energy production. Therefore, a 1-D photonic crystal, or Bragg stack, with a primary reflection band in the sub-bandgap range will not suffice for this application due to the additional reflection at wavelengths in the useful part of the spectrum.[21] For the sunlight with energy greater than the bandgap of the solar cell, the photonic mirror should instead provide an antireflective effect that allows more light into the cell compared to a reference module, improving energy output from the cell.

A second challenge of photonic mirror design is omnidirectionality. While an ideal photonic mirror would operate with perfect spectral selectivity at all angles of incidence, this is difficult to achieve in a practical photonic mirror design, and impossible in those based on layers of thin films. Real modules are of course installed in specific locations with varying direct

Received: December 22, 2017
Published: March 2, 2018

DOI: 10.1021/acsphotonics.7b01586
ACS Photonics XXXX, XXX, XXX−XXX

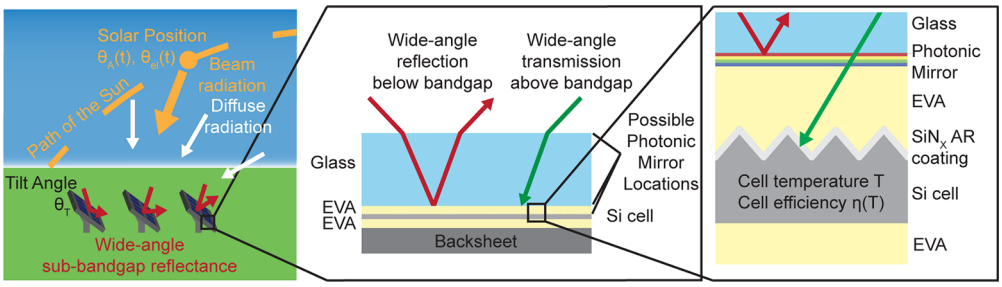

Figure 1. Design of the solar module integrated photonic mirrors accounts for both diffuse components of solar radiation (left) and the interface where the photonic mirror is present (middle) with the goal of reflecting sub-bandgap light while transmitting shorter-wavelength light. Simulations account for module properties including cell surface texture and changes in cell efficiency with temperature (right).

and diffuse components of the incident radiation depending on mounting and system design, and so not all angles of incidence are equally represented. For example, in a latitude-tilt module in Golden, Colorado, 22.4% of the energy arrives to the module at angles between 20° and 30° due to daily and seasonal variation in solar position. The peak occurs at 23°, equal to the tilt in Earth's axis. The photonic mirror therefore should not be designed for normal incidence, but to capture sunlight according to the actual angles of incidence present in a given application.

In this paper we identify the constraints on photonic mirror design based on aperiodic, one-dimensional layers of thin films. We first use an objective function to design the photonic mirror, which includes the expected energy received by a fixed-tilt module as a function of its angle of incidence, details of the AM1.5G[22] spectrum, and the Si cell internal quantum efficiency. After optimization via the objective function, photonic reflector designs are simulated in a previously developed self-consistent opto-electro-thermal model[20] under real weather and irradiance conditions derived either from measurement[23] or historical data[24] (Figure 1). We compare the performance relative to a baseline Si module, as shown in Figure 1, with ethylene-vinyl acetate (EVA) encapsulant, cover glass, and a standard antireflection coating (ARC) on top of the Si pyramids.

We examine the performance of photonic mirrors placed at different interfaces within the module and discuss their relative benefit from antireflection (optical) and cooling (thermal). We then consider the criterion of omnidirectionality, and show that a photonic reflector that increases solar module performance achieves its two functions regardless of the angle of incidence of radiation. The mirror must be created considering the full range of incident angles, but it does not have to perform equally well at all angles. Using this constraint, we construct photonic mirrors that achieve similar performance regardless of tilt angle or location (Golden, CO or Seattle, WA). Finally, we show that it is possible to optimize photonic mirrors with fewer than ten layers and create designs which improve the baseline module, especially when optimizing for the air/glass interface. These photonic mirrors generally act as antireflection coatings with a small thermal benefit, but may be easier to fabricate than more complex designs. A discussion of one such photonic mirror is provided in this paper.

METHODS

Solar Radiation. Our optimization scheme constructs photonic mirrors based on the amount of solar radiation received by the module at every angle of incidence. To determine these values, the solar position must be known. Solar azimuth angle (θ_a, degrees East of North) and zenith angle (θ_z, degrees) are calculated using the National Renewable Energy Laboratory (NREL) solar position algorithm[25] as a function of time and the module latitude, longitude, and altitude. Given the solar position vs time, the angle of incidence for beam radiation, θ_{AOI}, at a given moment is calculated using eq 1, where θ_t and θ_{am} are module tilt and module azimuth angles respectively, and t is the time. All modules considered here face due south, so θ_{am} is 180°.

$$\cos(\theta_{AOI}(t)) = \cos(\theta_z(t))\cos(\theta_t) + \sin(\theta_z(t))\sin(\theta_t)\cos(\theta_a(t) - \theta_{am}) \quad (1)$$

For photonic mirrors designed for Golden, CO, direct normal irradiance (DNI) vs time and diffuse horizontal irradiance (DHI) vs time data are taken from the NREL Solar Radiation Research Laboratory Baseline Measurement System (SRRL BMS)[23] at 1 min intervals from 00:00:00 on Jan. 1, 2015 to 23:59:00 on Dec. 31, 2015. For photonic mirrors optimized for other locations, DNI and DHI data are taken from Typical Meteorological Year data sets in the National Solar Radiation Data Base.[24] We use the 1991−2005 update: Typical Meteorological Year 3 (TMY3) data. The TMY3 DNI and DHI data are linearly interpolated onto 1 min intervals spanning the year from 00:00:00 on Jan. 1 to 23:59:00 on Dec. 31.

DNI and DHI irradiances are converted into energies incident on the plane of the module and split into beam and diffuse components. The beam energy, E_b, is calculated from DNI and θ_{AOI} using eq 2, where Δt is the time interval between data points (1 min). The diffuse energy, E_d, is calculated from DHI using the isotropic sky model,[26,27] shown in eq 3.

$$E_b(t) = \mathrm{DNI}(t)\cdot\cos(\theta_{AOI}(t))\Delta t \quad (2)$$

$$E_d(t) = \mathrm{DHI}(t)\cdot\frac{1 + \cos(\theta_t)}{2}\Delta t \quad (3)$$

Beam energies and diffuse energies as a function of time are then integrated to obtain energies as a function of angle of incidence upon the module. For the diffuse energy, we assume that the diffuse light is equally bright in all directions. Therefore, we assume that the distribution of diffuse energy as a function of angle of incidence is proportional to the sine of the angle of incidence times the cosine of the angle of incidence. The sine term arises from considering the fraction of the sky from which diffuse radiation is incident, and the cosine term arises from transposing to radiation through the plane of the module. We then ensure that eq 4 is satisfied, that is, the

DOI: 10.1021/acsphotonics.7b01586
ACS Photonics XXXX, XXX, XXX−XXX

total diffuse energy summed over angle is equal to the total diffuse energy summed over time.

$$\sum_{\theta} E_{\mathrm{d}}(\theta) = \sum_{t} E_{\mathrm{d}}(t) \tag{4}$$

Due to the range of incident angles we consider, beam energies at times when θ_{AOI} is greater than 90° are ignored. But, at those same times, the contribution of diffuse energy is considered. An overall energy versus angle of incidence curve equal to the sum of the curves for beam and diffuse energies is used to weight the reflection of a photonic mirror.

Optimization of Thin Film Mirrors. Aperiodic photonic thin-film mirrors are designed and simulated with the common dielectric materials SiO_2,[28] Si_3N_4,[29] TiO_2,[30] and Al_2O_3 (see Figure S1 in the Supporting Information). Superstrate and substrate indices for the cover glass and EVA are taken from refs 31 and 32, respectively, while for air we take $n = 1$. A given thin film reflector is characterized by calculating an objective function value, representing an estimate of the percentage optical improvement and percentage thermal improvement provided by the reflector. The objective function value is based on reflectivity calculations performed at wavelengths from 300 to 2200 nm and at angles of incidence at 1° intervals from 0° to 89°. If the superstrate material is not air, then angles of incidence are corrected using Snell's Law to match what they would be in the superstrate material. Reflection is then reported as a function of the free space angle of incidence. Reflection calculations are performed using the transfer matrix method.[33,34] We exclude wavelengths longer than 2200 nm because there is very little solar irradiation at these wavelengths. Although longer wavelengths are important for radiative cooling, bare photovoltaic cover glass[35] and stacks of dielectric layers[16] have been shown to have high emissivity. Further increasing this emissivity has a minor effect,[20] so we do not consider it in our optimization.

Objective function calculation begins by obtaining angle-weighted reflection values at each wavelength. The weighting for each angle is taken from the data of expected overall energy vs angle of incidence and normalized such that the weightings sum to unity (see Figures S2 and S3 in the Supporting Information). The reflection values at each angle are multiplied by the associated weight and summed to give one reflection value at each wavelength, $R_{\mathrm{w}}(\lambda)$. The objective function is based on both optical and thermal improvements compared to the baseline module. Baseline module properties are those based on weighted reflection values of the superstrate/substrate interface without the photonic reflector. Optical improvement is based on current generation, estimated using the transmission of light in the useful part of the spectrum (300−1100 nm), the internal quantum efficiency (IQE), and the spectral power in the AM1.5G spectrum ($P_{\mathrm{AM1.5}}$).

$$I = \int_{300}^{1100} (1 - R_{\mathrm{w}}(\lambda)) \cdot \lambda \cdot \mathrm{IQE}(\lambda) P_{\mathrm{AM1.5}}(\lambda) \mathrm{d}\lambda \tag{5}$$

The optical improvement is then given by eq 6, where I_{baseline} is the current expected in the baseline module.

$$\mathrm{opt}\%_{\mathrm{obj}} = 100\% \cdot (I/I_{\mathrm{baseline}} - 1) \tag{6}$$

The thermal improvement is based on the difference in sub-bandgap power reflected by the photonic mirror and the superstrate/substrate interface alone in the baseline module. The reflected power and the thermal improvement are calculated in eqs 7 and 8. In eq 8 we assume that a 30 W/m^2 increase in reflected power corresponds to a 1 K reduction in operating temperature. This figure is the result of previous observation of the ratio of waste heat generated to temperature rise above ambient in c-Si modules under 1000 W/m^2 illumination. It is used in the objective function for mirror design, but not in the full model as described in the next section. Additionally, we assume an 0.39% increase in efficiency per 1 K drop in temperature.[20] The objective function value is equal to the sum of the optical and thermal improvements.

$$P = \int_{1100}^{2200} R_{\mathrm{w}}(\lambda) P_{\mathrm{AM1.5}}(\lambda) \mathrm{d}\lambda \tag{7}$$

$$\mathrm{thermal}\%_{\mathrm{obj}} = \frac{P - P_{\mathrm{baseline}}}{30\,{}^{\mathrm{W}}/_{\mathrm{m^2K}}} \cdot 0.39\,{}^{\%}/_{\mathrm{K}} \tag{8}$$

An aperiodic photonic mirror is then produced using an optimization algorithm implemented in MATLAB based on the Nelder−Mead simplex algorithm.[36] The independent variables are the thicknesses of the layers in the thin film stack, which are optimized according to the objective function above. A simplex algorithm is not a gradient-based algorithm, and avoids finding the local minimum in the objective function when all layer thicknesses are set to zero. After layer thicknesses are optimized, a needle-insertion algorithm is used to determine the benefit of inserting an additional layer of any material in the structure.[34,37] After insertion of a new layer, the thicknesses of all layers are reoptimized, and needle insertion is repeated. This allows a complex structure to be built up from an initial structure of only a few layers. If an optimized structure contains a layer with less than 1 nm thickness, we delete the layer from the structure; the objective function is continuous with respect to deletion of very thin layers. Details of all photonic mirrors are available in Tables S1−S6 in the Supporting Information.

Opto-Electro-Thermal Simulations of Module Performance. Self-consistent opto-electro-thermal simulation of the photonic mirrors integrated into the module is carried out according to ref 20. Module optical properties, including module reflectance and absorption in each layer, are determined as functions of angle of incidence via a ray-tracing method capable of accounting for thin-film interference effects.[38,39] Module optical properties are then input to a time-dependent electrical and thermal model that calculates module cell temperature as a function of time and assumes a 17.1% efficiency at 298 K. The efficiency decreases by 0.39%/K increase in temperature. The ray-tracing simulation is capable of resolving the cell component in which energy is absorbed, including parasitic absorption, including the cell antireflection layer, the Si cell itself, and the metal contacts. However, in the thermal model, heat is injected uniformly to the cell layer. Given the high thermal conductivities and low thicknesses of the cell materials, the results are not sensitive to the exact location of parasitic absorption within the cell.[20] The thermal model includes radiative and convective heat exchange, and uses input weather data corresponding to 5 min intervals over the course of one year. Note that both daytime and nighttime are simulated. For photonic mirrors simulated in Golden, the weather data can be taken from ref 23. However, in this paper we also simulate photonic mirrors for Seattle, WA. The required weather inputs of wind speed and ambient temperature (dry bulb) are taken directly from TMY data corresponding to Seattle and linearly interpolated onto 5 min time intervals.[24] Beam and diffuse components of irradiance are

DOI: 10.1021/acsphotonics.7b01586
ACS Photonics XXXX, XXX, XXX−XXX

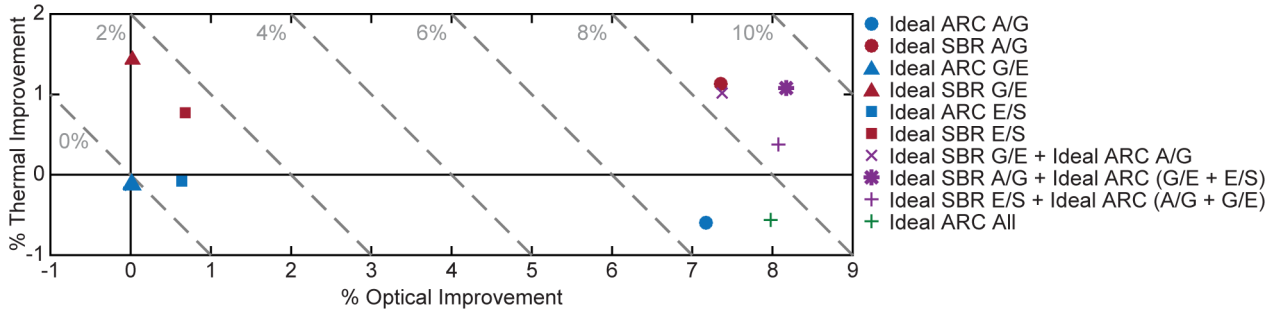

Figure 2. Properties of ideal photonic mirrors at various interfaces in the solar module. An ideal ARC has no reflection at any wavelength. An ideal SBR has unity reflection for sub-bandgap light and no reflection at shorter wavelengths. A/G is the air/glass interface. G/E is the glass/EVA interface. E/S is the EVA/Si interface (with pyramid surface texture). A "+" in the legend indicates the presence of a second or third photonic mirror at another interface.

taken from TMY data and transposed to plane-of-array irradiance using solar position angles calculated by the solar position algorithm and eqs 2 and 3.[25] Finally, sky and ground temperatures are estimated using TMY data for clearness index, dew point, ambient temperature (dry bulb), and global horizontal irradiance (GHI). Clearness index, K, is defined from eq 9, where ETHI is the calculated extraterrestrial horizontal irradiance, available in TMY data.

$$K = \frac{\text{GHI}}{\text{ETHI}} \tag{9}$$

Correlations for sky and ground temperature are discussed further in the Supporting Information, in Figure S4. The correlations were created by fitting similar irradiance, temperature, and dew point data to measured values for sky and ground temperature.[23]

Optical and thermal advantages for a photonic mirror simulated over a full year are extracted from raw simulation results. As with the objective function calculation, optical and thermal advantages extracted from simulation are determined relative to a baseline module that does not have the photonic mirror. Raw simulation results include time series of module output power and module temperature at 5 min intervals over one year, including overnight when no power is produced. To find relative optical and thermal improvement from simulation, first relative output power and relative temperature are calculated over time using eqs 10 and 11, where T is temperature and W is output power. The subscript refers to the data for the baseline module, and relative values are preceded by a Δ.

$$\Delta T(t) = T(t) - T_{\text{baseline}}(t) \tag{10}$$

$$\Delta W(t) = W(t) - W_{\text{baseline}}(t) \tag{11}$$

Power increase due to a thermal advantage (ΔW_{T}) is then calculated over time using the module temperature difference and the temperature coefficient of 0.39%/K.

$$\Delta W_{\text{T}}(t) = \Delta T(t) \cdot 0.39\,{}^{\%}\!/_{\text{K}} \cdot W_{\text{baseline}}(t) \tag{12}$$

Power increase due to an optical advantage (ΔW_{O}) is the difference between the total power change and the thermal advantage.

$$\Delta W_{\text{O}}(t) = \Delta W(t) - \Delta W_{\text{T}}(t) \tag{13}$$

Finally, the simulated optical improvement and thermal improvements are given by the sum over all time of the either the optical advantage or the thermal advantage divided by the sum of baseline power.

$$\text{opt\%}_{\text{sim}} = 100\% \cdot \frac{\sum_t \Delta W_{\text{O}}(t)}{\sum_t W_{\text{baseline}}(t)} \tag{14}$$

$$\text{thermal\%}_{\text{sim}} = 100\% \cdot \frac{\sum_t \Delta W_{\text{T}}(t)}{\sum_t W_{\text{baseline}}(t)} \tag{15}$$

Note that these summations are equivalent to numerical integrals of the power over time to yield energy. However, since the 5 min timesteps are constant and equivalent between the time points in the simulation, the value of the time step cancels out in the division.

While it is beyond the scope of this paper to address the applicability of the model to modules with noncrystalline Si-based photovoltaic cells, a change in the modeled cell materials only requires a change in the material properties or module geometry which appear as parameters in the current model, for example, bandgap wavelength, temperature coefficient, thermal conductivity, refractive index, cell thickness, cell surface texturing, and so on. So, the model can be adapted to other cell technologies. Finally, we note that while our model is similar to others,[40−46] we acknowledge the assumption in both the simulation and objective function that the incident spectrum is always proportional to the AM1.5G spectrum, and that a spectral correction is possible.[47−49]

RESULTS AND DISCUSSION

Properties of Ideal Photonic Mirrors. We first consider where the photonic mirror should be placed within the module by comparing idealized photonic mirrors, including ideal antireflection coatings, ideal sub-bandgap reflectors (SBR), and various combinations. While these photonic mirrors have properties that are not physically attainable, they represent boundaries on the best possible performance offered by a photonic mirror at a particular module interface. An individual mirror does not have to accomplish all of the benefits simultaneously, as the mirrors at different interfaces could be designed cooperatively. Photonic mirrors could be placed on the outside of the glass (air/glass interface or AG), within the module between the glass and the EVA encapsulant (glass/EVA interface or GE), or between the encapsulant and the solar cell (EVA/solar cell interface or ES). At the ES interface, the photonic mirror replaces the 75 nm SiN_x antireflection layer in the baseline module. We have previously considered the performance of an ideal SBR, ideal ARC, and the combination

DOI: 10.1021/acsphotonics.7b01586
ACS Photonics XXXX, XXX, XXX−XXX

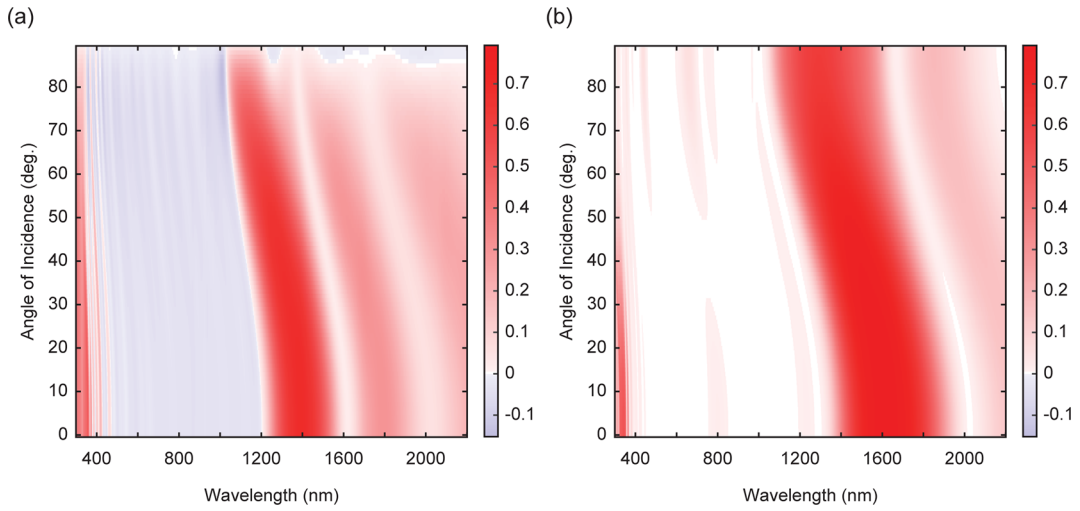

Figure 3. (Left) Net reflection from photonic mirror AG1 at the air/glass interface. (Right) Net reflection from photonic mirror GE1 at the glass/EVA interface. Blue shades indicate a reduction in reflection, the module with the photonic mirror reflects less light at that wavelength and angle than the module without. Red shades indicate increased reflection due to the photonic mirror.

of an ideal SBR and ideal ARC in these modules, but not the explicit design criteria for mirrors at each interface.[20]

A given photonic mirror's performance is compared to a baseline case with no photonic mirror, so the properties of the existing interfaces within the module determine the potential for benefit due to a photonic mirror. At the air/glass interface, there is reflection of ∼4% at normal incidence that could be eliminated with a photonic mirror. Indeed, commercial solar modules often use antireflection coatings on the top glass to reduce this reflection.[50] In contrast, the glass/encapsulant interface in the interior of the module has very low reflectivity, <0.1% across almost all wavelengths, so no photonic mirror at this interface would be able to provide significant antireflection over the baseline module. Additionally, even though these effects are not simulated in this work, photonic mirrors at the air/glass interface are exposed to weathering and damage. This can affect performance of the photonic mirror; mirrors interior to the module are protected from damage.

Results of the ideal photonic mirror simulations are given in Figure 2, showing the simulated relative percent optical improvement against the simulated percent thermal improvement, predicted from a full year of weather and irradiance conditions in Golden, CO. Immediately, a difference in performance depending on the interface and type of photonic mirror is apparent. At the air/glass interface, the antireflection provided by either an ideal SBR (red circle) or ideal ARC (blue circle) provides a >7% optical benefit. However, for the ideal ARC, there is a thermal penalty of ∼0.6%; the module with the ARC operated at hotter temperatures than the baseline module. The thermal penalty is due to the transmission of additional light with energies both higher and lower than the bandgap. For energies less than the bandgap, the additional light directly heats the module. For energies greater than the bandgap, the additional transmitted light causes additional current to be produced by the module, which leads to additional waste heat from thermalization, and therefore higher module temperatures. Therefore, for any antireflection coating, there will be some thermal penalty due to the additional current generated compared to baseline.

An ideal SBR, however, does offer a thermal benefit since it reflects all of the sub-bandgap radiation. The greatest thermal benefit is possible at the glass/EVA interface (∼1.4%, red triangle), because the glass and EVA in the baseline module are nearly index-matched, and the interface is very transmissive. Therefore, adding a SBR at this interface leads to greater gain compared to the reference module than placing the SBR at an interface with lower baseline transmissivity, such as the air/glass interface. Furthermore, while the high transmissivity limits the optical benefit available via antireflection, it also limits the thermal penalty due to additional current generation. At the air/glass interface, the ideal SBR retains the optical improvement of the ideal ARC, but has a smaller thermal benefit (∼1.1%) than the ideal SBR at the at the glass/EVA interface due to the additional baseline reflection from the reference case.

While we do not optimize explicit photonic mirrors for the EVA/Si solar cell interface, we have run simulations of ideal cases. The baseline module contains a 75 nm SiN_x antireflection layer on top of a pyramidal surface texture of the cell, both of which affect the results of the ideal case simulations. Those simulations, then, report on possible improvements over the existing antireflection coating. The 75 nm SiN_x layer is already very effective, with the ideal ARC (blue square) and ideal SBR (red square) providing only an ∼0.6−0.7% optical improvement, and the ideal SBR giving an ∼0.8% thermal improvement. We note both that there is some improvement possible at this interface, and that any designs will have to consider the existing pyramid surface texture of the cell.

Finally, ideal photonic mirrors could be incorporated at multiple interfaces. In this approach, only a single SBR is beneficial, as the sub-bandgap light only needs to be reflected once, but incorporation of ARCs at other interfaces offers additional benefit. For example, a module with a spectrally selective photonic mirror at the glass/EVA interface would also benefit from the addition of an antireflection coating at the air/glass interface. In the case of an ideal SBR at the glass/EVA interface and an ideal ARC at the air/glass interface (purple x-mark), simulation results indicate similar performance to an ideal SBR at the air/glass interface, with a slightly smaller thermal benefit in the former due perhaps to sub-bandgap absorption in the glass. Similarly, placing the ideal SBR at the EVA/Si cell interface (purple plus sign) has a smaller thermal benefit due to absorption of the sub-bandgap light in upper

DOI: 10.1021/acsphotonics.7b01586
ACS Photonics XXXX, XXX, XXX−XXX

layers of the module. With ideal ARCs at all interfaces, the maximum optical benefit can be achieved, ~8%, with a thermal penalty of ~0.6% for the reasons mentioned above (green plus sign). The best possible module, however, would be in the case of an ideal SBR at the air/glass interface, and ideal ARCs at other interfaces (purple star). The ideal SBR at the air/glass interface reflects sub-bandgap light away before it reaches any other interfaces, and the module has a ~1.1% thermal improvement in addition to the ~8% optical improvement offered by antireflection.

Photonic Mirrors the Air/Glass and Glass/EVA Interfaces. Photonic mirrors comprised of one-dimensional layers of real materials were then constructed using the optimization routine. These mirrors exhibit realistic spectral and angular performance. Mirrors were constructed for the air/glass interface (photonic mirror AG1) and the glass/EVA (photonic mirror GE1) interface. The initial structure for both AG1 and GE1 was five periods of a quarter-wave Bragg stack targeted for maximum reflection at 1250 nm. These photonic mirrors were optimized and simulated using weather and irradiance data assuming a latitude-tilt module in Golden, CO (39.742 N, 105.179 W). In addition, we simulated a commercial antireflection coating (glass ARC) both on its own at the air/glass interface, and in conjunction with photonic mirror GE1. The glass ARC is a 99 nm porous SiO_2 layer, as described in section 3.2 of ref 51.

Figure 3a,b show net reflection at all wavelengths and angles of incidence from photonic mirrors AG1 and GE1, respectively. Net reflection is the difference between the reflection of the particular interface with and without the photonic mirror. Blue-shaded areas are regions of reduced reflection, while red-shaded areas are regions where there is additional reflection compared to the bare interface. Note that for both AG1 and GE1, the center wavelength of the reflection band at normal incidence shifted from the initial design wavelength of 1250 nm to ~1400 nm for AG1 and ~1600 nm for GE1. This ensured that there are no angles of incidence for which light with energy greater than the bandgap is strongly reflected. Additional reflection at longer wavelengths in both structures is attributed to side lobes remaining from the reflection spectrum of the initial Bragg stack. The reflection band at less than 400 nm in both structures is attributed to a harmonic of the main reflection band also present in the initial structure which was not completely suppressed by the aperiodicity introduced during structure optimization.

Aside from the harmonic reflection band, in the range 300–1100 nm reflection is very low at all angles in both structures. For AG1, reflection is low enough to provide antireflection at most useful wavelengths and most angles since the air/glass interface itself is reflective. At normal incidence, air/glass reflectivity is 4%, rising to ~10% at 60° and ~40% at 80°. However, even though reflection from GE1 is very low in the useful range, it is not low enough to provide substantial antireflection compared to the glass/EVA interface. Again, since the glass and EVA are nearly index-matched, reflection is less than 0.1% at normal incidence across all wavelengths, and never more than 0.5% at any wavelength or angle of incidence, which limits the potential optical benefit of photonic mirrors at that interface and places a strict standard for breaking even optically. Figure S5 in the Supporting Information shows reflectance from the air/glass and glass/EVA interfaces. While thermal benefit is still possible at the glass/EVA interface, it must outweigh the likely optical detriment to produce a net energy improvement. At normal incidence, integration of the reflection spectrum shows that AG1 reflects 41.8 W/m^2 sub-bandgap power while GE1 reflects 53.6 W/m^2, both out of 174 W/m^2 sub-bandgap power incident upon the structure.

Full-year simulations were then run using these two photonic mirrors to find the optical improvement, thermal improvement, and overall energy output improvement. These results are also compared to the estimates of the optical improvement and thermal improvement obtained from the objective function calculation alone (Figure 4). Due to the antireflection provided

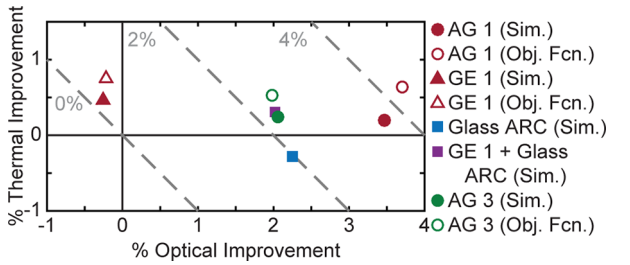

Figure 4. Objective function (Obj. Fcn.) values and simulation (Sim.) results for mirrors AG1, GE1, and AG3. The Glass ARC is a 99 nm porous SiO_2 antireflection coating shown in ref 50 and is placed at the Air/Glass interface. "GE1 + Glass ARC" is a simulation with both GE1 at the Glass/EVA interface and the Glass ARC at the Air/Glass interface.

by AG1, both the objective function (red empty circle) and the simulation (red filled circle) give a large optical benefit and a small thermal benefit (3.44% and 0.2% for the simulation), although these are both considerably smaller than the ideal case (7.36% and 1.13%, respectively, from simulation). For GE1, however, both the objective function (empty red triangle) and simulation (red filled triangle) give a small optical detriment (−0.29% from simulation) since the photonic mirror is still slightly more reflective than the glass/EVA interface in the region from 300−1100 nm. For the glass ARC simulation (blue filled square), there is an optical improvement of ~2% and a thermal penalty of −0.3% (compared to 7.17% and −0.6% for the ideal ARC). When acting in tandem with GE1 (purple filled square), the glass ARC provides the optical benefit (slightly reduced by the presence of GE1) and GE1 provides the thermal benefit. The largest thermal benefit is found for the GE1 case, the largest overall benefit is found for the AG1 case due to the antireflection improvement, and GE1 with a glass ARC provides a compromise.

The objective function calculation and the full simulation are consistent but there is a disagreement of ~0.4% absolute for AG1 and ~0.3% absolute for GE1. We offer two possible explanations for the disagreement. For AG1, since there is optical improvement, in the full opto-electro-thermal simulation the additional useful light passed by the photonic mirror will create additional waste heat as well since the module is not simulated as 100% efficient. The additional waste heat raises the temperature of the module and partially offsets the benefit of sub-bandgap reflectance, since in the simulation the thermal benefit is calculated based on module temperature and not reflectance.[20] For GE1, since the photonic mirror is behind an air/glass interface, the spectrum of sunlight reaching the photonic mirror at the glass/EVA interface differs from the AM1.5G spectrum. The objective function does not account for this. Sunlight incident at oblique angles is less likely to reach the glass/EVA interface than sunlight incident at near-normal

DOI: 10.1021/acsphotonics.7b01586
ACS Photonics XXXX, XXX, XXX−XXX

angles due to the difference in reflectivity of the air/glass interface. The irradiance reaching the glass/EVA interface is biased toward near-normal angles of incidence, where the reflection band of the photonic mirror is red-shifted to a wavelength range with less spectral power than wavelengths closer to the bandgap. A photonic mirror at the glass/EVA interface in the simulation will thus reflect less sub-bandgap power than predicted by the objective function, and therefore, the simulated thermal benefit will be lower.

Effect of Changing Module Tilt Angle and Geographic Location. We next consider the omnidirectionality of the mirror. The main challenge in creating photonic mirrors based on one-dimensional layers is the changing reflectivity with angle of incidence, as the reflection values will significantly increase and blue shift at oblique angles. However, not all angles are represented equally in the spectrum. Figure 5a shows the fraction of total energy received at each angle by a module in Golden at latitude tilt, a tilt angle of 30° and a tilt angle of 20°. Lower-than-latitude-tilt angles are typically used in large solar arrays or in areas where space is constrained to prevent one module from shading another.[52] At latitude tilt, the angle of incidence of beam radiation with the module is lowest near the equinoxes. At lower tilts, the beam radiation comes at the lowest angles in the summer and higher angles in other seasons. The peak angle is no longer 23°, but instead shifts to higher angles: 32° at 30° tilt and 42° at 20° tilt. Secondary peaks show up at lower angles as well: 13° at 30° tilt and 3° at 20° tilt in Golden, CO.

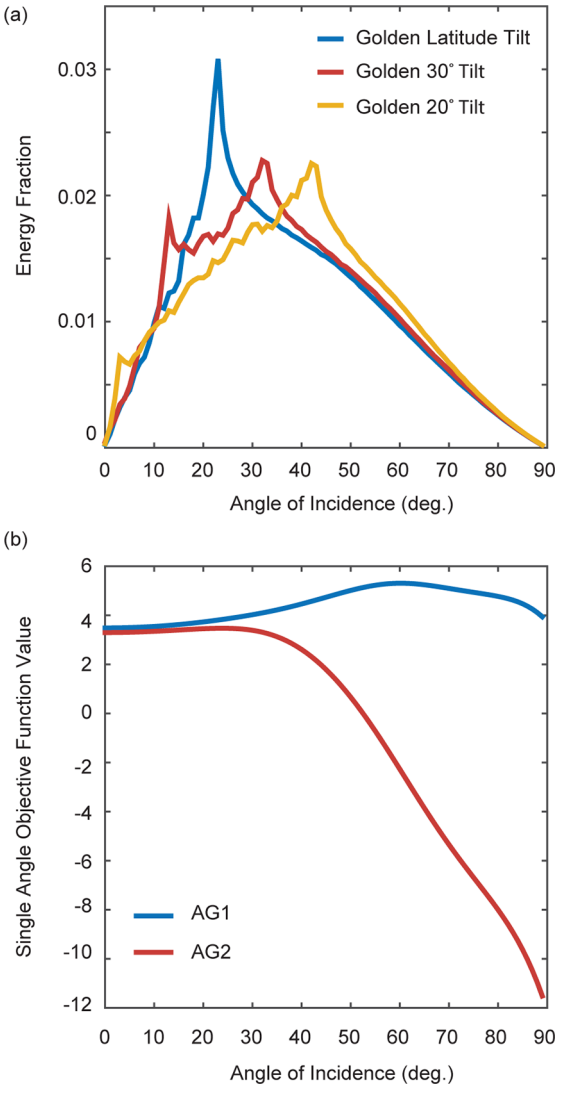

Figure 5. (a) Comparison of the fraction of expected energy on a module in Golden, CO at latitude tilt, 30° tilt, and 20° tilt. (b) The objective function of photonic mirrors AG1 and AG2 evaluated separately at each angle.

We compare two different photonic mirrors: AG1, which was constructed considering the relative amounts of energy incident at all angles, and photonic mirror AG2 which is an intentionally suboptimal structure constructed considering only reflection at 23°, beginning with the same initial structure as AG1. Figure 5b shows the objective function values for photonic mirrors AG1 and AG2 considering only one angle at a time. For photonic mirror AG1, peak performance occurs under illumination at 60°, and there are no angles where AG1 is detrimental. However, for photonic mirror AG2, peak performance occurs near 23° incidence, the only angle for which reflection was considered during optimization. For angles closer to normal incidence, the performance of AG2 remains beneficial, but at angles higher than 23° the performance decreases, becoming detrimental under illumination at angles greater than 50°. A net reflection plot for photonic mirror AG2 (Figure S6 in the Supporting Information) shows that its reflection band is red-shifted compared to that of AG1, such that the reflection band edge is at 1100 nm at 23°. The poor objective function value is entirely due to reflection of light at wavelengths shorter than 1100 nm for angles greater than 23°.

Given that AG1 is a more omnidirectional mirror, it performs well as the tilt angle is lowered. A change in module tilt angle changes the peak angles at which radiation is received. Table 1 shows the results from the full simulation, which indicate that the optical improvement is slightly enhanced as the module tilt is lowered for 20° tilt. The thermal benefit declines slightly at all conditions other than the optimization condition and is slightly worse at 30° tilt than at 20° tilt.

These results indicate that, despite the presence of peaks in the radiation at specific angles, a one-dimensional photonic mirror based on layers of thin films should not be designed for the peak angle. For these mirrors, the blue shift of reflection features with increasing angle of incidence means that if a reflection band in a structure is placed to reflect the most sub-bandgap light at 23° incidence (as in the latitude tilt case) while not reflecting light with energy greater than the bandgap, blue shift of the reflection band will decrease module performance for light incident at higher angles. A substantial portion of the spectrum is incident at higher angles. For the air/glass interface, the baseline reflection increases from ∼4% at normal incidence to over 20% at higher angles, and so the antireflective behavior of the photonic mirror at high angles can also lead to better performance. The harmonic reflection band is also blue-shifted at steep angles, which reduces reflection in the wavelength range from 300 to 400 nm and improves antireflection.

To better understand the role of radiation from all angles, we study the performance of the mirror under diffuse light and beam light separately. Figure 6a shows a scatter plot of the time series simulation results for photonic mirror AG1 in Golden, CO. Each dot represents a single 5 min time step in the simulation; only daytime data are shown, excluding twilight periods. The scatter plots show the total advantage, the sum of the simulated optical and thermal advantages at that time point, against the beam angle of incidence, calculated for that time

DOI: 10.1021/acsphotonics.7b01586
ACS Photonics XXXX, XXX, XXX−XXX

Table 1. Simulation Results for Photonic Mirror AG1 in Golden, CO with Varying Module Tilt Angles, Photonic Mirror AG1 on a Latitude Tilt Module in Seattle, WA, and Photonic Mirror AG2 in Golden, CO on a Latitutde Tilt Module[a]

photonic mirror	AG1				AG2
optimization location/tilt angle	Golden, CO latitude	Golden, CO latitude	Golden, CO latitude	Golden, CO latitude	Golden, CO latitude
simulation location/tilt angle	Golden, CO latitude	Golden, CO 20°	Golden, CO 30°	Seattle, WA latitude	Golden, CO latitude
% optical improvement	3.44	3.55	3.42	3.43	2.03
% thermal improvement	0.20	0.15	0.13	0.12	0.22
% total improvement	3.64	3.70	3.55	3.55	2.25

[a]Also included is the performance of AG1 at its design condition in Golden at latitude tilt.

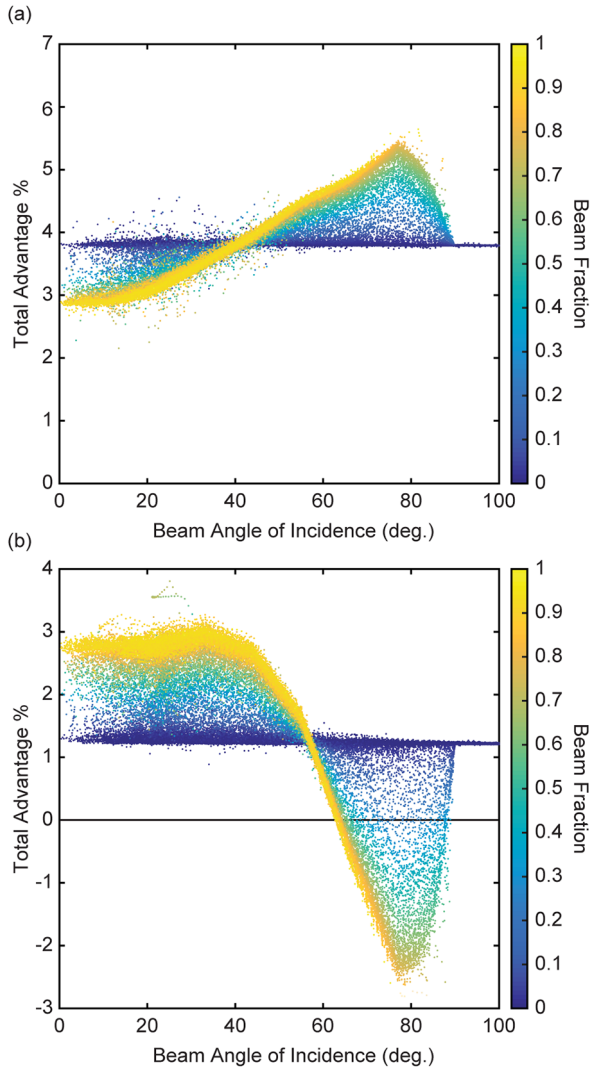

Figure 6. Scatter plot of simulated percentage power increase relative to baseline versus the beam angle of incidence (eq 1) for (a) AG1 and (b) AG2. Each dot represents a 5 min daytime interval in the simulation, excluding twilight periods. The dots are colored according to the fraction of the plane-of-array incidence coming from the solar beam. Blue colors signify nearly 100% diffuse light, yellow colors signify nearly 100% beam light. When the beam angle of incidence is greater than 90°, the sun does not shine on the front of the module, and all incident light is diffuse. About 28% of the points have a beam fraction greater than 0.8 and about 43% have a beam fraction less than 0.2.

from eq 1. Each dot is colored by the fraction of plane of array irradiance received by the module at that time point attributable to beam radiation. Blue colored dots correspond to times with nearly zero beam radiation, or nearly 100% diffuse radiation, while yellow colored dots correspond to times with nearly 100% beam radiation. A beam angle of greater than 90° indicates that the beam radiation is located behind the module. This condition dictates that 100% of the incident light is diffuse.

A difference in performance under beam and diffuse light is apparent. When the beam fraction is low and most of the plane of array irradiance is diffuse, the module performance is always the same, regardless of the beam angle of incidence. Diffuse radiation is incident with at least some energy at each angle of incidence, so the performance under diffuse radiation depends on reflectivity at all angles of incidence. Under beam radiation, however, the module performance increase due to the photonic mirror depends on the beam angle of incidence. As was predicted by the objective function calculations shown in Figure 5b, better performance is achieved under high angles of incidence than low angles of incidence, even though AG1 was constructed with a peak in energy received at 23°.

Figure 6b shows the same scatter plot with data corresponding to photonic mirror AG2. As with AG1, the performance under diffuse light is constant regardless of the beam angle of incidence and the performance under beam light depends on its angle of incidence. However, AG2 performs worse under beam illumination at more oblique angles than it does at near normal angles, again due to reflection of light with energies above the bandgap at high angles. And, because of this detrimental reflection, performance under diffuse light is reduced for AG2 relative to AG1. Full simulation results, shown in Table 1, indicate that a module with photonic mirror AG2 produces 1.5% less energy than a module with photonic mirror AG1.

To further examine the omnidirectionality of optimized photonic mirrors, we consider a change in the physical location of the module. Photonic mirror AG1 was originally optimized for and simulated in a latitude-tilt module in Golden, CO. However, irradiance conditions vary from location to location. Seattle, WA, for example, has many more cloudy days than Golden (mean annual clearness index 0.462 for Seattle vs 0.618 for Golden),[53] and receives a greater fraction of its sunlight as diffuse radiation rather than beam radiation.

A change in geographic location while maintaining latitude module tilt results primarily in a change in the fraction of all light received that is diffuse. Figure S3 in the Supporting Information shows the fraction of energy received at each angle for a latitude tilt module in Golden and Seattle. The fraction of diffuse light increases from 32.7% in Golden to 38.7% in Seattle. Photonic mirror AG1 was simulated using weather and irradiance data corresponding to a latitude-tilt module in Seattle, the result is in Table 1. The optical improvement for AG1 in Seattle is reduced only 0.01% compared to Golden, and the thermal improvement is reduced by 0.08%.

Mirrors AG1 and AG2 are different in that AG1 was designed considering the full range of incident angles, as

DOI: 10.1021/acsphotonics.7b01586
ACS Photonics XXXX, XXX, XXX−XXX

opposed to just one angle for AG2. The performance difference between AG1 and AG2 is much greater than performance differences that arise due to a change in tilt angle or geographic location. Therefore, we stress the importance in general of considering angle of incidence when creating spectrally selective photonic structures for module cooling.

An optimal photonic mirror will be omnidirectional in the sense that it will provide a net benefit for incident light at every angle. The photonic mirror does not have to be equally beneficial at all angles, nor most beneficial at peak angles of incidence. Since the photonic mirror performs differently at each angle of incidence, changing the location (the amount of diffuse light received) or the tilt angle (angles of peak energy) will only slightly change the overall performance benefit. Even if the module were placed in a location with very little diffuse light, consideration of more oblique angles of incidence is still necessary for beam radiation, as ∼20% of the beam energy is incident at angles greater than 50°.

One motivation for designing a photonic mirror considering only one angle of incidence, as in the case of AG2, is that it may be possible at that angle to achieve significantly higher performance than for a mirror like AG1 which considers all angles. Our results, however, suggest that this is not the best strategy. In both objective function calculations (Figure 5b) and simulation results for high beam fraction conditions (Figure 6a,b), photonic mirrors AG1 and AG2 perform similarly at low angle, until diverging around 23° where performance of AG2 begins to decrease. Despite only taking into account 23° incidence, AG2 does not have better performance at that angle than does AG1. This suggests that there is no compromise between achieving excellent low angle and high angle performance simultaneously.

Performance of Photonic Mirrors with Few Layers. In photonic mirrors AG1 and GE1, the initial condition for optimization was a Bragg stack, which required several 2-layer periods to create a reflection band. However, for photonic mirror AG1, its primary effect was antireflection of light in the 300−1100 nm range. The possibility is considered, then, of creating photonic mirrors with only a few layers without a reflection band, but still with excellent antireflection between 300 and 1100 nm. We optimized a new photonic mirror at the air/glass interface for Golden, CO at latitude tilt. Photonic mirror AG3 was constructed with an initial condition of just two layers, one Al_2O_3 layer on top of one Si_3N_4 layer and both with the same optical thickness as the layers in the initial condition of AG1. Layer thickness optimization and needle insertion were performed and a 10-layer structure was created. Since AG2 is not built based on a Bragg stack, the thermal benefit of the structure was given additional weighting in the objective function to ensure that some thermal benefit is achieved.

Figure 7 shows the net reflection from photonic mirror AG3 and Figure 4 shows results of a simulation of a latitude-tilt module with photonic mirror AG3 in Golden (green circles). The net reflection plot shows that while there is not a reflection band as in the Bragg stack based structures, there is still significant sub-bandgap reflection. At normal incidence, 40.6 W/m^2 is reflected at wavelengths longer than the bandgap. At higher angles, photonic mirror AG3 begins to reflect useful radiation between 1000 and 1100 nm, which was avoided in the more complex structures. While the 2% optical benefit of photonic mirror AG3 is slightly less than the optical benefit of the glass ARC, AG3 provides a thermal benefit that the glass

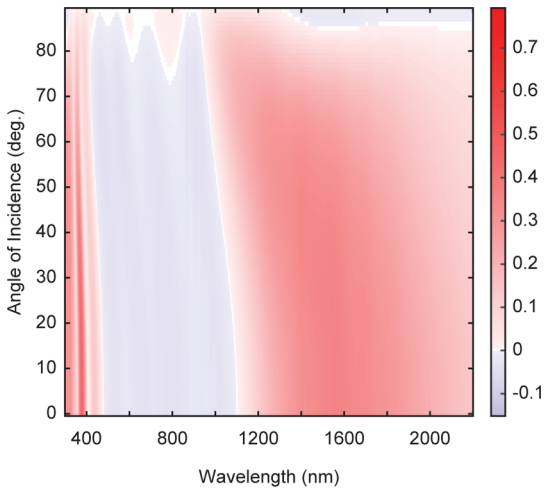

Figure 7. Net reflection from the photonic mirror AG3 at the air/glass interface. Blue shades indicate a reduction in reflectance: the module with the photonic mirror reflects less light at that wavelength and angle than the module without. Red shades indicate increased reflection due to the photonic mirror.

ARC does not, meaning that both antireflection and module temperature reduction are achieved. In fact, the ARC causes a thermal detriment to energy yield, which is turned into a benefit with AG3, a more sophisticated design accounting for sub-bandgap radiation. While photonic mirror AG3 does not perform as well as photonic mirror AG1, its advantage lies in the relatively simple structure and potential ease of fabrication.

CONCLUSIONS

This paper examines aperiodic photonic reflectors for integration into solar modules. These coatings act to reflect radiation with energies too low to be useful for photocurrent generation, preventing parasitic absorption of that radiation, cooling the module, and extending its service life.[20] At the top interface between air and glass, there is the possibility for antireflection of useful shortwave light, while maintaining or improving reflection of sub-bandgap light. Photonic mirrors between the glass and encapsulant still have the potential to reflect sub-bandgap light, but will likely not offer any antireflection, since the reflection at that interface is already extremely low. Our photonic mirror at the air/glass interface is able to provide antireflection and a small thermal benefit, increasing module energy by 3.7% compared to the baseline with no photonic mirror. By providing both increased photocurrent and module temperature reduction, our photonic mirrors are also an improvement over traditional ARCs, which increase module temperature and potentially decrease module lifetime.[20] Enhanced performance is possible at the interface between the glass and encapsulant; however, the thermal benefit must outweigh any penalty due to increased reflection of useful light. Our photonic mirror at that interface offers a 0.18% increase in energy; however, in conjunction with a traditional antireflection photonic mirror at the top interface, this performance could be improved further. While the results shown here are specific to crystalline Si modules, the general findings for mirror design criteria (omnidirectionality and placement within the laminate) are applicable to other materials systems.

Excellent photonic mirror performance is achieved when reflection at all angles of incidence is taken into account during

DOI: 10.1021/acsphotonics.7b01586
ACS Photonics XXXX, XXX, XXX−XXX

construction of the mirror. The resulting mirror is omnidirectional in that it provides a net benefit under illumination at all angles. By following this guideline, a change in tilt angle or location does not significantly impact the performance of our photonic mirror. Finally, while we primarily constructed photonic mirrors based off of an initial starting Bragg stack structure, it is possible to start with much simpler initial conditions and achieve successful photonic mirrors with a relatively low layer count. Such photonic mirrors are worth considering for their ease of fabrication.

■ ASSOCIATED CONTENT

Supporting Information

The Supporting Information is available free of charge on the ACS Publications website at DOI: 10.1021/acsphotonics.7b01586.

Refractive index of modeled materials, changes in angle weighting due to module tilt angle and geographic location, full materials and thicknesses of each mirror, sky temperature and ground temperature calculations (PDF).

■ AUTHOR INFORMATION

Corresponding Author

*E-mail: veferry@umn.edu.

ORCID

Vivian E. Ferry: 0000-0002-9676-6056

Notes

The authors declare no competing financial interest.

■ ACKNOWLEDGMENTS

The authors thank Dana Dement for providing Al_2O_3 optical data. We thank the Department of Energy Solar Energy Technologies Office for funding through the Solar Graduate Research Internship program hosted at the National Renewable Energy Laboratory. This work was partially supported by the University of Minnesota. This work was supported by the U.S. Department of Energy under Contract No. DE-AC36-08GO28308 with Alliance for Sustainable Energy, LLC, the Manager and Operator of the National Renewable Energy Laboratory. Funding provided by U.S. Department of Energy, Office of Energy Efficiency and Renewable Energy Solar Energy Technologies Office. The U.S. Government retains and the publisher, by accepting the article for publication, acknowledges that the U.S. Government retains a nonexclusive, paid-up, irrevocable, worldwide license to publish or reproduce the published form of this work, or allow others to do so, for U.S. Government purposes.

■ REFERENCES

(1) Sun, X.; Silverman, T. J.; Zhou, Z.; Khan, M. R.; Bermel, P.; Alam, M. A. Optics-Based Approach to Thermal Management of Photovoltaics: Selective-Spectral and Radiative Cooling. *IEEE J. Photovolt.* **2017**, *7* (2), 566−574.

(2) Dupré, O.; Vaillon, R.; Green, M. A. Temperature Coefficients of Photovoltaic Devices. In *Thermal Behavior of Photovoltaic Devices*; Springer, 2017.

(3) Siecker, J.; Kusakana, K.; Numbi, B. P. A Review of Solar Photovoltaic Systems Cooling Technologies. *Renewable Sustainable Energy Rev.* **2017**, *79*, 192−203.

(4) Shukla, A.; Kant, K.; Sharma, A.; Biwole, P. H. Cooling Methodologies of Photovoltaic Module for Enhancing Electrical Efficiency: A Review. *Sol. Energy Mater. Sol. Cells* **2017**, *160*, 275−286.

(5) Hasanuzzaman, M.; Malek, A. B. M. A.; Islam, M. M.; Pandey, A. K.; Rahim, N. A. Global Advancement of Cooling Technologies for PV Systems: A Review. Sol. *Sol. Energy* **2016**, *137*, 25−45.

(6) Shukla, A.; Kant, K.; Sharma, A.; Biwole, P. H. Cooling Methodologies of Photovoltaic Module for Enhancing Electrical Efficiency: A Review. *Sol. Energy Mater. Sol. Cells* **2017**, *160*, 275−286.

(7) Ballif, C.; Dicker, J.; Borchert, D.; Hoffmann, T. Solar Glass with Industrial Porous SiO2 Antireflection Coating: Measurements of Photovoltaic Module Properties Improvement and Modelling of Yearly Energy Yield Gain. *Sol. Energy Mater. Sol. Cells* **2004**, *82* (3), 331−344.

(8) Du, Y.; Le, N. C. H.; Chen, D.; Chen, H.; Zhu, Y. Thermal Management of Solar Cells Using a Nano-Coated Heat Pipe Plate: An Indoor Experimental Study. *Int. J. Energy Res.* **2017**, *41*, 867−876.

(9) Kafafi, Z. H.; Martin-Palma, R. J.; Nogueira, A. F.; O'Carroll, D. M.; Pietron, J. J.; Samuel, I. D. W.; So, F.; Tansu, N.; Tsakalakos, L. The Role of Photonics in Energy. *J. Photonics Energy* **2015**, *5* (1), 050997.

(10) Karthik, D.; Pendse, S.; Sakthivel, S.; Ramasamy, E.; Joshi, S. V. High Performance Broad Band Antireflective Coatings Using a Facile Synthesis of Ink-Bottle Mesoporous MgF2 Nanoparticles for Solar Applications. *Sol. Energy Mater. Sol. Cells* **2017**, *159*, 204−211.

(11) Liu, L.-Q.; Wang, X.-L.; Jing, M.; Zhang, S.-G.; Zhang, G.-Y.; Dou, S.-X.; Wang, G. Broadband and Omnidirectional, Nearly Zero Reflective Photovoltaic Glass. *Adv. Mater.* **2012**, *24* (47), 6318−6322.

(12) Sandhu, S.; Yu, Z.; Fan, S. Photon Management for Enhanced Open-Circuit Voltage in Nanostructured Solar Cells. *J. Phys. D: Appl. Phys.* **2015**, *48* (41), 413001.

(13) Sargunanathan, S.; Elango, A.; Mohideen, S. T. Performance Enhancement of Solar Photovoltaic Cells Using Effective Cooling Methods: A Review. *Renewable Sustainable Energy Rev.* **2016**, *64*, 382−393.

(14) San Vincente, G.; Bayon, R.; German, N.; Morales, A. Long-Term Durability of Sol−gel Porous Coatings for Solar Glass Covers. *Thin Solid Films* **2009**, *517* (10), 3157−3160.

(15) Wehrspohn, R. B.; Upping, J. 3D Photonic Crystals for Photon Management in Solar Cells. *J. Opt.* **2012**, *14*, 024003.

(16) Li, W.; Shi, Y.; Chen, K.; Zhu, L.; Fan, S. A Comprehensive Photonic Approach for Solar Cell Cooling. *ACS Photonics* **2017**, *4*, 774−782.

(17) Zhu, L.; Raman, A.; Fan, S. Radiative Cooling of Solar Absorbers Using a Visibly Transparent Photonic Crystal Thermal Blackbody. *Proc. Natl. Acad. Sci. U. S. A.* **2015**, *112* (40), 12282−12287.

(18) Zhu, L.; Raman, A.; Wang, K. X.; Anoma, Ma. A.; Fan, S. Radiative Cooling of Solar Cells. *Optica* **2014**, *1* (1), 32−38.

(19) Hu, M.; Pei, G.; Li, L.; Zheng, R.; Li, J.; Li, J. Theoretical and Experimental Study of Spectral Selectivity Surface for Both Solar Heating and Radiative Cooling. *Int. J. Photoenergy* **2015**, *2015*, 1.

(20) Silverman, T. J.; Deceglie, M. G.; Subedi, I.; Podraza, N. J.; Slauch, I. M.; Ferry, V. E.; Repins, I. Reducing Operating Temperature in Photovoltaic Modules. *IEEE J. Photovolt.* **2018**, *8* (2), 532−540.

(21) Brovelli, L. R.; Keller, U. Simple Analytical Expressions for the Reflectivity and the Penetration Depth of a Bragg Mirror between Arbitrary Media. *Opt. Commun.* **1995**, *116*, 343−350.

(22) ASTM G173-03(2012), *Standard Tables for Reference Solar Spectral Irradiances: Direct Normal and Hemispherical on 37° Tilted Surface*, ASTM International, West Conshohocken, PA, 2012

(23) Stoffel, T.; Andreas, A. NREL Solar Radiation Research Laboratory (SRRL): Baseline Measurement System (BMS). *Dataset NREL/DA-5500−56488*; National Renewable Energy Laboratory: Golden, CO, United States, 1981.

(24) Wilcox, S.; Marion, W. *Users Manual for TMY3 Data Sets, Dataset NREL/TP-581−43156*; National Renewable Energy Laboratory: Golden, CO, United States, 2008.

(25) Reda, I.; Andreas, A. Solar Position Algorithm for Solar Radiation Applications. *Technical Report NREL/TP-560−34302*; National Renewable Energy Laboratory: Golden, CO, United States, 2008.

DOI: 10.1021/acsphotonics.7b01586
ACS Photonics XXXX, XXX, XXX−XXX

(26) Loutzenhiser, P. G.; Manz, H.; Felsmann, C.; Strachan, P. A.; Frank, T.; Maxwell, G. M. Empirical Validation of Models to Compute Solar Irradiance on Inclined Surfaces for Building Energy Simulation. Sol. *Sol. Energy* **2007**, *81*, 254−267.
(27) Shukla, K. N.; Rangnekar, S.; Sudhakar, K. Comparative Study of Isotropic and Anisotropic Sky Models to Estimate Solar Radiation Incident on Tilted Surface: A Case Study for Bhopal, India. *Energy Rep.* **2015**, *1*, 96−103.
(28) *Optical Data from Sopra SA, Dataset*; Software Spectra, Inc.
(29) Luke, K.; Okawachi, Y.; Lamont, M. R. E.; Gaeta, A. L.; Lipson, M. Broadband Mid-Infrared Frequency Comb Generation in a Si3N4Microresonator. *Opt. Lett.* **2015**, *40* (21), 4823−4826.
(30) Davis, K. O.; Jiang, K.; Habermann, D.; Schoenfeld, W. V. Tailoring the Optical Properties of APCVD Titanium Oxide Films for All-Oxide Multi-Layer Anti-Reflection Coatings. *IEEE J. Photovolt.* **2015**, *5* (5), 1265−1270.
(31) *Refractive Index Library, Material: Glass, Low-Fe Sodalime [Pil], Dataset*; PV Lighthouse.
(32) Vogt, M. R.; Holst, H.; Schulte-Huxel, H.; Blankemeyer, S.; Witteck, R.; Hinken, D.; Winter, M.; Min, B.; Schinke, C.; Ahrens, I.; et al. Optical Constants of UV Transparent EVA and the Impact on the PV Module Output Power under Realistic Irradiation. *Energy Procedia* **2016**, *92*, 523−530.
(33) Born, M.; Wolf, E. *Principles of Optics*, 6th ed.; Pergamon Press, 1980.
(34) Griesmann, U. *Optical Thin Film Toolbox for Octave and MATLAB*, 2015.
(35) Gentle, A.; Smith, G. Is Enhanced Radiative Cooling of Solar Cell Modules Worth Pursuing? *Sol. Energy Mater. Sol. Cells* **2016**, *150*, 39−42.
(36) Nelder, J. A.; Mead, R. A Simplex Algorithm for Function Minimization. *Comput. J.* **1965**, *7* (4), 308−313.
(37) Tikhonravov, A. V.; Trubetskov, M. K.; DeBell, G. W. Application of the Needle Optimization Technique to the Design of Optical Coatings. *Appl. Opt.* **1996**, *35* (28), 5493−5508.
(38) Subedi, I.; Silverman, T. J.; Deceglie, M. G.; Podraza, N. J. *Impact of Infrared Optical Properties on Crystalline Si and Thin Film CdTe Solar Cells*, 2017.
(39) Dupré, O.; Vaillon, R.; Green, M. A. *Thermal Behavior of Photovoltaic Devices: Physics and Engineering*; Springer International Publishing: Cham, 2017.
(40) Edgar, R.; Stachurski, Z.; Cochard, S. Optimising Direct Normal Insolation of Rectangular PV Platforms. *Sol. Energy* **2016**, *136*, 166−173.
(41) Han, K.; Chang, C.-H. Numerical Modeling of Sub-Wavelength Anti-Reflective Structures for Solar Module Applications. *Nanomaterials* **2014**, *4*, 87−128.
(42) Hassabou, A.; Abotaleb, A.; Abdallah, A. Passive Thermal Management of Photovoltaic Modules-Mathematical Modeling and Simulation of Photovoltaic Modules. *J. Sol. Energy Eng.* **2017**, *139*, 061010.
(43) Huh, D.; Shin, J.-H.; Byun, M.; Son, S.; Jung, P.-H.; Choi, H.-J.; Kim, Y.-D.; Lee, H. Analysis of Long-Term Monitoring Data of PV Module with SiOx-Based Antireflective Patterned Protective Glass. *Sol. Energy Mater. Sol. Cells* **2017**, *170*, 33−38.
(44) Lee, Y.; Tay, A. A. O. Finite Element Thermal Analysis of a Solar Photovoltaic Module. *Energy Procedia* **2012**, *15*, 413−420.
(45) Long, Y. Optimizing One-Dimensional Photonic-Crystals Based Semitransparent Organic Solar Cells by Tailoring Reflection Phase Shift within Photonic Bandgap. *Appl. Phys. Lett.* **2011**, *99*, 093310.
(46) McColl, S. J.; Rodgers, P.; Eveloy, V. Thermal Management of Solar Photovolatics Modules for Enhanced Power Generation. Renew. *Renewable Energy* **2015**, *82*, 14−20.
(47) Krin, B.; Topic, M. Diffuse and Direct Light Solar Spectra Modeling in PV Module Performance Rating. *Sol. Energy* **2017**, *150*, 310−316.
(48) Ernst, M.; Holst, H.; Winter, M.; Altermatt, P. P. SUNCALCULATOR: A Program to Calculate the Angular and Spectral Distribution of Direct and Diffuse Solar Radiation. *Sol. Energy Mater. Sol. Cells* **2016**, *157*, 913−922.
(49) Boden, S. A.; Bagnall, D. M. Sunrise to Sunset Optimization of Thin Film Antireflective Coatings for Encapsulated, Planar Silicon Solar Cells. *Prog. Photovoltaics* **2009**, *17*, 241−252.
(50) *Photon Management in Solar Cells*; Wehrspohn, R. B., Rau, U., Gombert, A., Eds.; Wiley-VCH: Weinheim, 2015.
(51) Vogt, M. R. Development of Physical Models for the Simulation of Optical Properties of Solar Cell Modules. *Ph.D. Thesis*, Leibniz University of Hanover: Hanover, Germany, 2015.
(52) Passias, D.; Kallback, B. Shading Effects in Rows of Solar Cell Panels. Sol. *Sol. Cells* **1984**, *11*, 281−291.
(53) Knapp, C. L.; Stoffel, T. L.; Whitaker, S. D. Insolation Data Manual: Long-Term Monthly Averages of Solar Radiation, Degree-Days and Global KT for 248 National Weather Service Stations. *Data Manual SERI/SP-755−789*; Solar Energy Research Institute: Golden, CO, United States, 1980.

NOTE ADDED AFTER ASAP PUBLICATION

This paper was originally published ASAP on March 13, 2018. Table S3 in the Supporting Information was corrected, and the revised version was reposted on March 14, 2018.

DOI: 10.1021/acsphotonics.7b01586
ACS Photonics XXXX, XXX, XXX−XXX